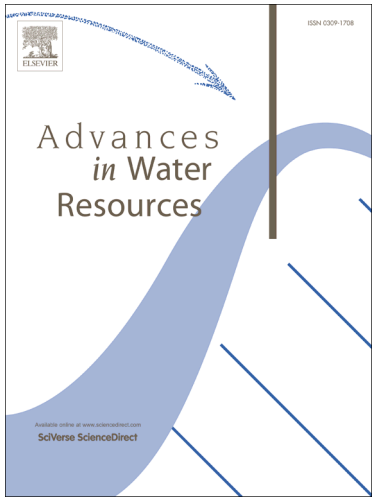

A new lattice Boltzmann model for interface reactions between immiscible fluids

Paolo Roberto Di Palma, Christian Huber, Paolo Viotti

PII: S0309-1708(15)00094-9
DOI: http://dx.doi.org/10.1016/j.advwatres.2015.05.001
Reference: ADWR 2372

To appear in: *Advances in Water Resources*

Received Date: 30 October 2014
Revised Date: 29 April 2015
Accepted Date: 2 May 2015

Please cite this article as: Di Palma, P.R., Huber, C., Viotti, P., A new lattice Boltzmann model for interface reactions between immiscible fluids, *Advances in Water Resources* (2015), doi: http://dx.doi.org/10.1016/j.advwatres.2015.05.001

"A new lattice Boltzmann model for interface reactions between immiscible fluids"

Di Palma Paolo Roberto[*a,b], Huber Christian[c] and Viotti Paolo[a]

(a) Department of Civil, Building and Environmental Engineering, Sapienza University of Rome, Via Eudossiana 18, 00184-Rome, Italy paolo.viotti@uniroma1.it
(b) IRSA-CNR Water Research Institute - National Research Council, Via Salaria km 29.300, Monterotondo (Rome), Italy dipalma@irsa.cnr.it
(c) School of Earth and Atmospheric Sciences, Georgia Institute of Technology, Atlanta, 30332 GA, USA christian.huber@eas.gatech.edu

Abstract

In this paper, we describe a lattice Boltzmann model to simulate chemical reactions taking place at the interface between two immiscible fluids. The phase-field approach is used to identify the interface and its orientation, the concentration of reactant at the interface is then calculated iteratively to impose the correct reactive flux condition. The main advantages of the model is that interfaces are considered part of the bulk dynamics with the corrective reactive flux introduced as a source/sink term in the collision step, and, as a consequence, the model's implementation and performance is independent of the interface geometry and orientation. Results obtained with the proposed model are compared to analytical solution for three different benchmark tests (stationary flat boundary, moving flat boundary and dissolving droplet). We find an excellent agreement between analytical and numerical solutions in all cases. Finally, we present a simulation coupling the Shan Chen multiphase model and the interface reactive model to simulate the dissolution of a collection of immiscible droplets with different sizes rising by buoyancy in a stagnant fluid.

Keywords

Reactive multiphase flow, Lattice Boltzmann method, Interface reactions, Groundwater remediation

I. Introduction

Mass exchange of a non-aqueous phase liquid (commonly referred to as "NAPL") in groundwater represents an important two-phase problem in environmental engineering. These contaminants have a low solubility and act as a long-term source of contamination. There are two classes of NAPL compounds: light ("LNAPLs") and dense NAPLs ("DNAPLs") according to their density relative to water [1, 2]. LNAPLs float on the groundwater table moving in the same direction as the hydraulic gradient while DNAPLs sink down to the bedrock of the aquifer or remain trapped in low permeability lenses [1, 2].

With the increase of pollution cases by NAPLs, several techniques of groundwater remediation have been developed, including flushing, air sparging, chemical oxidation, thermal treatment and bioremediation [3, 4]. These techniques focus on the separate-phase source reduction, increasing

[*] Corresponding author.
Email: dipalma@irsa.cnr.it (Paolo Roberto Di Palma)

the extraction and treatment of dissolved plume. Even with the development of these strategies, the remediation of sites contaminated by NAPLs remains difficult and not efficient. The general approach is to enhance the dissolution of the NAPL at the interface with the aqueous phase, and reduce the contamination source longevity. Recent studies [5, 6] showed that the pollutants mass transfer is limited by mixing of contaminants and injected/added compound (air, microorganism or chemicals according to the different remediation method). Forecasting the duration of the remediation procedure to remove totally the contaminant mass flux from the source zone is of particular importance to design an effective and cost-conscious strategy.

Numerical models that simulate the cleanup and dissolution of the invading pollutants have been widely used over the last few years to study and design remediation [7-14], however most existing models do not account for the dynamic interphase mass transfer associated with NAPL dissolution. Most numerical models are set at the field scale (or Darcy scale), based on continuum assumptions, with a grid spacing on the order of meters [15, 16]. In these models, the properties of the medium are assumed homogeneous within a representative elementary volume ("REV") and do not account for the dynamics that takes place at the pore-scale, as such, they tend to overestimate the dissolution rate of contaminants as reported by several authors [6, 17].

On the other end of the spectrum, pore-scale models are able to capture physicochemical processes associated with mass transport and chemical reactions, as well as the pore-scale velocity field from Navier-Stokes equations ("NSE") at the cost of large computational demands. Over the last decades, Lattice Boltzmann Models ("LBM") have been widely used for their capability to simulate meso-scale and micro-scale phenomena. Lattice Boltzmann models solve the discretized Boltzmann equation and can be used to recover partial differential equations such as Navier-Stokes equations and the advection-diffusion/dispersion equation ("ADE") [18-22]. The LBM consist of the evolution of a series of pseudo-particles, which can propagate (stream) over a discrete lattice and collide with each other, conserving mass and momentum at each node of the lattice. Compared to traditional computational fluid dynamics methods, LBM are well-suited for the fluid and transport dynamics in complex geometries (e.g. porous media) because of its ability to (1) introduce simple rules for complex boundary conditions, (2) compute chemical gradients locally, and its efficiency for parallelization [18-23].

Different studies have focused on the development of boundary conditions for surface reaction in ADE with LBM. Kang at al. [24-26] proposed to introduce heterogeneous reactions at the interface between fluid and solid nodes as internal boundary conditions. Chen and Zhang [27] extended the method of Kang to simulate diffusion from liquid carbon-dioxide droplets to seawater. Walsh and Saar [28] proposed an interpolated lattice Boltzmann boundary condition to introduce first-order reaction kinetics and, recently, Zhang et al. [29], Chen et al. [30] and Gillisen [31] suggested a halfway bounce-back scheme to implement the concentration or thermal boundary conditions and surface reactions between fluid and solid phases, based on the scheme developed by Ladd [32]. Finally Chen et al. [33] use a mixed scheme for reactive boundary condition, coupling the boundary treatment studied by Kang [26] and Zhang [29] (Eq. 33 (a,b) in [33]) to overcome the issue for moving boundary and yielding a similar scheme obtained by Walsh and Saar [28], but suitable to simulate all types of boundary conditions.

In this work, we propose an alternative method also based on the LBM. The model is based on the phase-field approach [34, 35] and requires information from nearest neighbors around the interface, which avoids the necessity to calculate the normal to the interface. Our model is therefore

independent of interface shape and orientation, which becomes advantageous when dealing with complex time-dependent interfaces. The mathematical description of the model is provided in section II, it is followed by validations in section III. Specifically, we test our model with analytical and numerical solution over different scenarios (flat boundary, moving boundary and dissolving droplet). Section IV provides a discussion of the performance of our model. In section V, we present a simulation of multiphase reactive transport of multiple droplets ascending buoyantly in a fluid at rest to showcase the ability of the model to handle complex geometries.

II. Model Description

1. Lattice Boltzmann for fluid flow

The lattice Boltzmann method is based on the discrete kinetic equation:

$$f_i(x + e_i\Delta x, t + \Delta t) = f_i(x,t) + \Omega_i\big(f(x,t)\big), \qquad (1)$$

where f_i represents the particle distribution function traveling along the *ith* direction with velocity e_i; $\Omega_i\,(f(x,t))$ is the collision operator which represents the rate of change of f_i resulting from collisions between particles. Δt and Δx are time and space increments, respectively, and both equal to one, $\mathbf{e_i}$ are the local particle velocities that constrain the motion of particles on the lattice. Starting from an initial state, the configuration of particles at each time step evolves according to two sequential sub-steps, (a) streaming, where particles move to the nearest node along the velocity vector $\mathbf{e_i}$, and (b) collision, which occurs when particles arriving at a node interact and exchange momentum to relax to a local equilibrium.

For our fluid dynamics calculations, we use a 2 dimensional square lattice with eight nearest neighbors, labeled D_2Q_9 (see Fig. 1a) [19, 20, 22, 36].

The collision operator Ω_i is often linearized following the assumption of Bathnagar-Gross-Krook ("BGK") or single relaxation time ("SRT") because it provides a simple and computationally efficient numerical scheme [18, 36]. However, as reported by several authors, a multiple relaxation time approach ("MRT") can be used instead and allows for higher order boundary conditions and improved stability [38, 39]. The BGK collision is defined as:

$$\Omega_i = -\frac{1}{\tau}(f_i(x,t) - f_i^{eq}(x,t)), \qquad (2)$$

where τ is the relaxation time and $f_i^{eq}(x,t)$ is the local equilibrium distribution function which is obtained from a second order Taylor expansion of Maxwell-Boltzmann's distribution with respect to the local macroscopic velocity field $\boldsymbol{u}$:

$$f_i^{eq}(x,t) = \rho\omega_i\left[1 + 3\frac{e_i\cdot u}{c_s^2} + \frac{9}{2}\frac{(e_i\cdot u)^2}{c_s^4} + \frac{3}{2}\frac{u^2}{c_s^4}\right] \qquad (3)$$

with the lattice weights:

$$\omega_i = \begin{cases} \frac{4}{9} & i = 0 \\ \frac{1}{9} & i = 1,2,3,4 \\ \frac{1}{36} & i = 5,6,7,8 \end{cases}$$

and c_s^2 is the sound speed, equal to 1/3, for D2Q9 lattice topology.

The macroscopic variables, the local fluid density ρ and fluid velocity $\mathbf{u}$=(u,v) are given by:

$$\rho = \sum_{i=0}^{8} f_i\,, \qquad \rho\mathbf{u} = \sum_{i=0}^{8} \boldsymbol{e_i} f_i. \qquad (4)$$

Using a Chapman-Enskog expansion, the Navier-Stokes equations can be derived from the Eq. (1) [19, 20, 22, 36]:

$$\frac{\partial \rho}{\partial t} + \nabla \cdot (\rho \boldsymbol{u}) = 0$$

$$\frac{\partial \rho \boldsymbol{u}}{\partial t} + \mathrm{u}\nabla \cdot (\rho \boldsymbol{u}) = -\nabla \mathrm{p} + \nabla \cdot (\rho \nu \nabla \boldsymbol{u}), \quad (5)$$

where the kinematic viscosity is defined as $\nu = c_s^2(\tau - \frac{1}{2})\Delta t$.

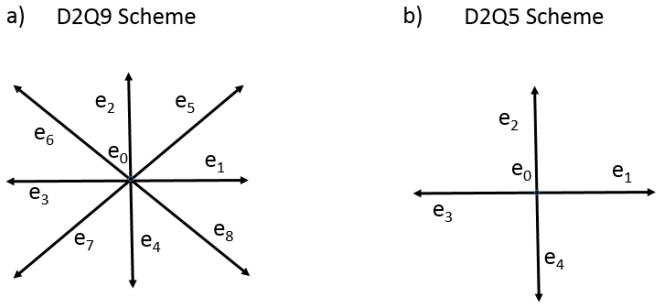

Fig. 1. Lattice topologies and lattice velocity indexing for the D2Q9 (a) and D2Q5 (b).

2. Lattice Boltzmann for advection-diffusion (or solute transport)

The LB equation for reactive transport obeys a similar rule as the fluid solver:

$$g_i(x + e_i\Delta x, t + \Delta t) = g_i(x,t) + \Omega_i\big(g(x,t)\big) \qquad (6)$$

We use a D_2Q_5 lattice topology (Fig. 1b), which requires less storage memory, but is limited to smaller Peclet number values compared to the D2Q9 lattice [26]. The collision operator in equation (7) is also reduced to a single relaxation time BGK operator:

$$\Omega_i = -\frac{1}{\tau}(g_i(x,t) - g_i^{eq}(x,t)). \qquad (7)$$

We use linear equilibrium functions g_i^{eq} to solve for the advection-diffusion equation for solvents:

$$g_i^{eq} = w_i C(1 + 3\mathbf{e_i} \cdot \mathbf{u}) \qquad (8)$$

The D_2Q_5 lattice weights are w_0=1/3 and $w_{1,\dots,4}$=1/6, and $\mathbf{u}$ is the local velocity field, calculated with the fluid dynamics solver. The local concentration is $C = \sum_{i=0}^{4} f_i$, and the relaxation time τ_s is related to the diffusion coefficient D by:

$$D = c_s^2(\tau_s - \frac{1}{2})\Delta t. \qquad (9)$$

The advection diffusion equation can be retrieved by a Chapman-Enskog expansion from Eq. (6) [36, 40]:

$$\frac{\partial C}{\partial t} + \nabla \cdot (C\boldsymbol{u}) = \nabla \cdot (D\nabla C). \qquad (10)$$

3. Interface reaction kinetics

Homogeneous chemical reactions [24-26, 35-36, 41-42] are often introduced in the LB equation (7) as source/sink terms S_i. Heterogeneous (or interface) reactions are generally implemented as internal boundary conditions, i.e. sites that evolve according to a different dynamical rule than the bulk [24-26]. In this work, we propose a different approach in which the classic LBM algorithm (streaming and collision steps) is computed at each point of the domain, including interfaces between different phases/components, and heterogeneous reactions only occur at interfaces following a phase-field approach [34, 35]. This phase-field approach requires a flag variable $\varepsilon(x,t)$ that is defined as 0 or 1 depending if the node is occupied by phase 1 or 2 (for a two components system).

In a previous work [36], the flag variable was used in the collision step to identify the sites where the reactions occurred. In this study, our goal is to develop a simple approach that does not depend on the interface geometry to implement reactions between two moving immiscible fluids. We identify the position of the interface with the phase-field variable between the streaming step and the collision. We then calculate the mass flux across the interface before the collision and correct it to satisfy the mass balance condition:

$$-D\nabla_n C = k_r C_0 (C - C_0)^m = \Phi_R, \qquad (11)$$

where $\nabla_n C$ is the concentration normal to the interface, k_r is the reaction rate, C_0 is the equilibrium or saturation concentration and m is the order of reaction (we only considered first order reactions in this study).

Using the phase-field method, the direction n normal to the interface is obtained when $\varepsilon(\mathbf{x}, t) = 0$ and there is one or more direction i such that $\varepsilon(\mathbf{x} + \mathbf{e}_i, t) = 1$. Using the D_2Q_5 lattice, the normal direction can match with one of the main directions ($\mathbf{e}_{1,..,4}$)(as shown in Fig. 2(a,b)) or diagonal when a staircase approximation exists. In this case the mass flux is split/projected along the x,y directions (Fig. 2(b)).

One of the advantages of the LBM resides in its ability to compute the mass flux locally. In the case of pure diffusion (no advective flux), the concentration gradient ($\nabla_n C$) can be retrieved by:

$$\nabla_n C = \frac{\sum_i (\varepsilon(\boldsymbol{x}+\boldsymbol{e_i}) - \varepsilon(\boldsymbol{x})) e_i g_i^{(1)}}{-\tau c_s^2 \Delta t} \qquad (12)$$

where $g_{i,n}^{(1)} = (\varepsilon(\boldsymbol{x}+\boldsymbol{e_i}) - \varepsilon(\boldsymbol{x}))(g_i - g_i^{(eq)})$ represents the non-equilibrium part of the particle distribution function traveling along the normal to the interface (assuming a staircase approximation), which can be calculated before the collision step.

Combing equation (11)-(12) yields:

$$\sum_i e_i g_{i,n}^{(1)} = \frac{k_r C_0 (C - C_0)}{D} \tau c_s^2 \Delta t = \Phi_R. \qquad (13)$$

We can now enforce the proper reaction condition at interfaces by replacing the non-equilibrium part of the distribution function in the direction normal with $\tilde{g}_{i-n}^{(1)}$:

$$\tilde{g}_{i,n}^{(1)} = g_{-(i,n)}^{(1)} + \Phi_R = g_{-(i,n)}^{(1)} + \frac{k_r C_0 (C - C_0)}{D} \tau c_s^2 \Delta t \qquad (14)$$

The macroscopic concentration at the current timestep *t*, is re-calculated using the new distributions $\tilde{g}_{i,n}^{(1)}$ and Eq. (13) and (14) are computed iteratively until the interface concentration converges. Once the model has converged, the mass balance (Eq. 11) and the interface concentration are both consistent and the collision step can be computed. The treatment of the interface is illustrated in Fig. 2a.

We can summarize the reaction scheme as follows: (1) the streaming step is performed at all nodes in the domain. (2) After the flag variable identifies the interface and orientation, the reactive/diffusive flux is calculated according to Eq. (13). (3) The distribution functions in the direction normal to the interface are updated with Eq. (14) iteratively until the interface concentration converges and, (4), the collision step is performed.

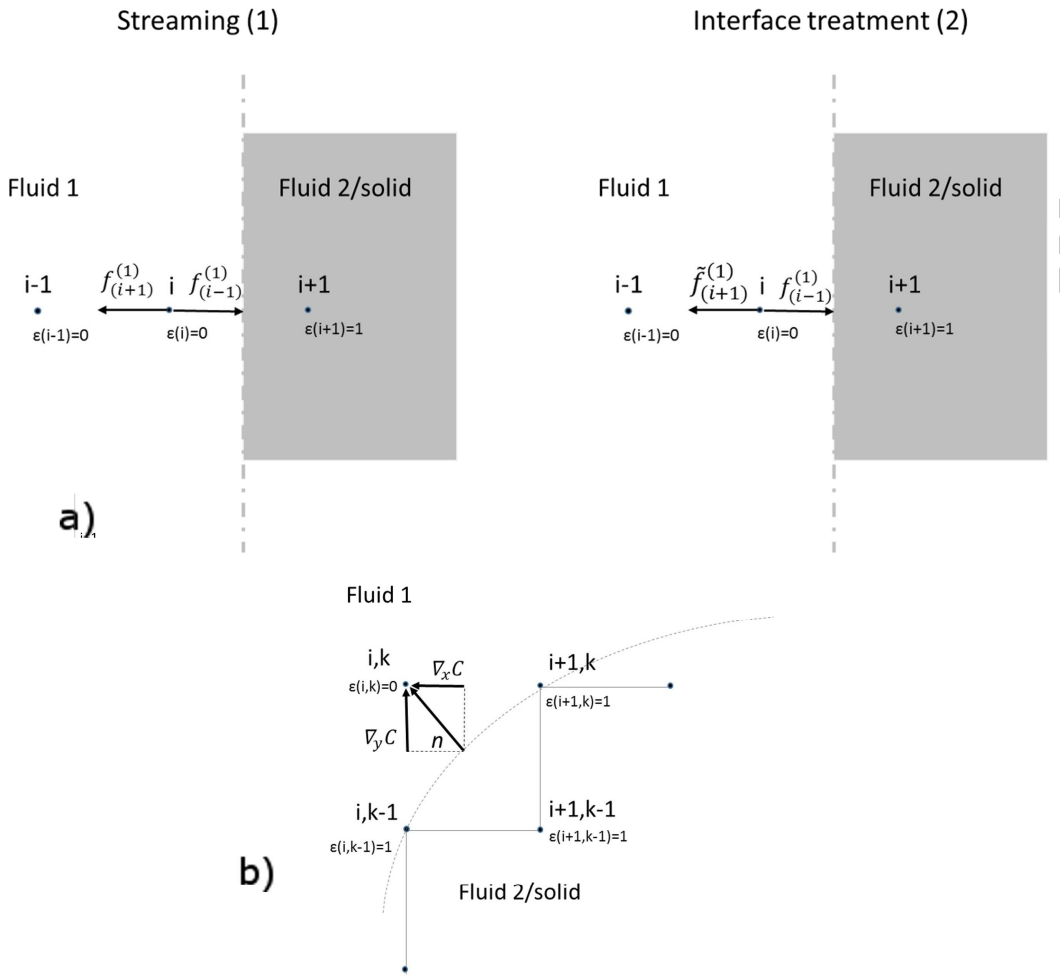

Fig. 2. (a) The reactive part of the model is calculated between the streaming step and the collision. The concentration gradient is calculated locally as $\nabla_n C = \frac{\sum_i e_i g_i^{(1)}}{-\tau c_s^2 \Delta t}$ and set equal to the reactive flux $\Phi_R = k_r C_0 (C - C_0)^m$. The unknown function distribution coming from the fluid 2/solid interface is found iteratively by setting $\tilde{g}_{(i+1)}^{(1)} = g_{(i-1)}^{(1)} + \Phi_R$. (b) Illustration of the normal-direction estimation with the phase field in case of staircase approximation.

The advantage of this scheme is that it can deal with moving interfaces with no additional correction because the advective flux is already considered in the equilibrium distributions. The linear equilibrium distribution function adds a spurious term in the Chapman-Enskog expansion (time derivative of the advective flux) in Eq. (3) according to Latt [44]. We found that, under all conditions tested here, the spurious term only plays a small role in the mass balance equation at the interface. However, it can be easily removed following the procedure described in [43, 44].

The main advantage of this kinetic reaction model lies in the approach to calculate the interface concentration. The interpolated scheme or the halfway bounce-back conditions generally use a finite-difference scheme to get the interface concentration required to calculate the reactive flux

[28, 29]. Other authors introduce the heterogeneous reaction as internal boundary conditions. This procedure is elegant, but the mass balance equation to solve at interface nodes differs from the bulk and depends on the orientation of the interface, and, as such, becomes more complex or computationally demanding in multicomponent systems with large effective surface area between the components [24-26, 33]. With the phase-field approach, the algorithm we propose does not use different closure equations depending on the orientation of the interface; additionally, moving interfaces can be naturally accounted for.

III. Results and discussion

In this section, we present the results obtained with different numerical simulations. Three different benchmark tests are presented to study the accuracy of the model. The reported test considers diffusion with a flat static interface, advection and diffusion with a flat moving boundary and surface evaporation out of a cylinder.

1. Flat static interface

The first test consists of a one-dimensional diffusive transport from a fixed (interface velocity $\mathbf{u}_w$=0) flat boundary with linear kinetics at the interface. We compared the LBM results to the analytical solution of Crank [48], used in Walsh and Saar [28]:

$$C(x,t) = C_0 + (C_{eq} - C_0) \times \left[erfc\left(\frac{x}{2\sqrt{Dt}}\right) - exp(hx + h^2 Dt) \times erfc\left(\frac{x}{2\sqrt{Dt}} + h\sqrt{Dt}\right)\right] \quad (15)$$

Where C_0 is the initial concentration, C_{eq} is the equilibrium/saturation concentration, $h = \frac{k_R}{D}$ and D is the diffusivity. The test was performed in a square domain (100x100 nodes) of height H=100 lattice units (l.u.) and length L=100 l.u.. For this simulation, the phase field variable is fixed as $\varepsilon\left(x \le \frac{L}{2}\right) = 1$ and $\varepsilon\left(x > \frac{L}{2}\right) = 0$, and the initial concentrations was set to C_0=$C_{eq} = 1$ when $\varepsilon(\boldsymbol{x}) = 1$ and $C_0 = 0$ for $\varepsilon(\boldsymbol{x}) = 0$. Lengths are normalized by the grid spacing and time is normalized so that dt= 1 in l.u..

A Dirichlet boundary condition is set at the left side of the domain (x=0), imposing the equilibrium concentration $C_{eq} = 1$. This condition is enforced by solving the missing part of the distribution functions [45, 46]:

$$g_1(x = 0, y, t) = C_{eq} - [g_0(x = 0, y, t) + g_2(x = 0, y, t) + g_3(x = 0, y, t) + g_4(x = 0, y, t)] \quad (16)$$

At the right side of the domain we impose a no-flux condition *(∂C/∂x=0)*:

$$g_3(x = L, y, t) = g_3(x = L - 1, y, t) \quad (17)$$

while periodic boundary condition are set on the top and bottom.

In Fig. 3 (a-d) we show the comparison between the analytical solution and our model results for different values of h at different times. We observe an excellent agreement between numerical results and the analytical solution in all cases.

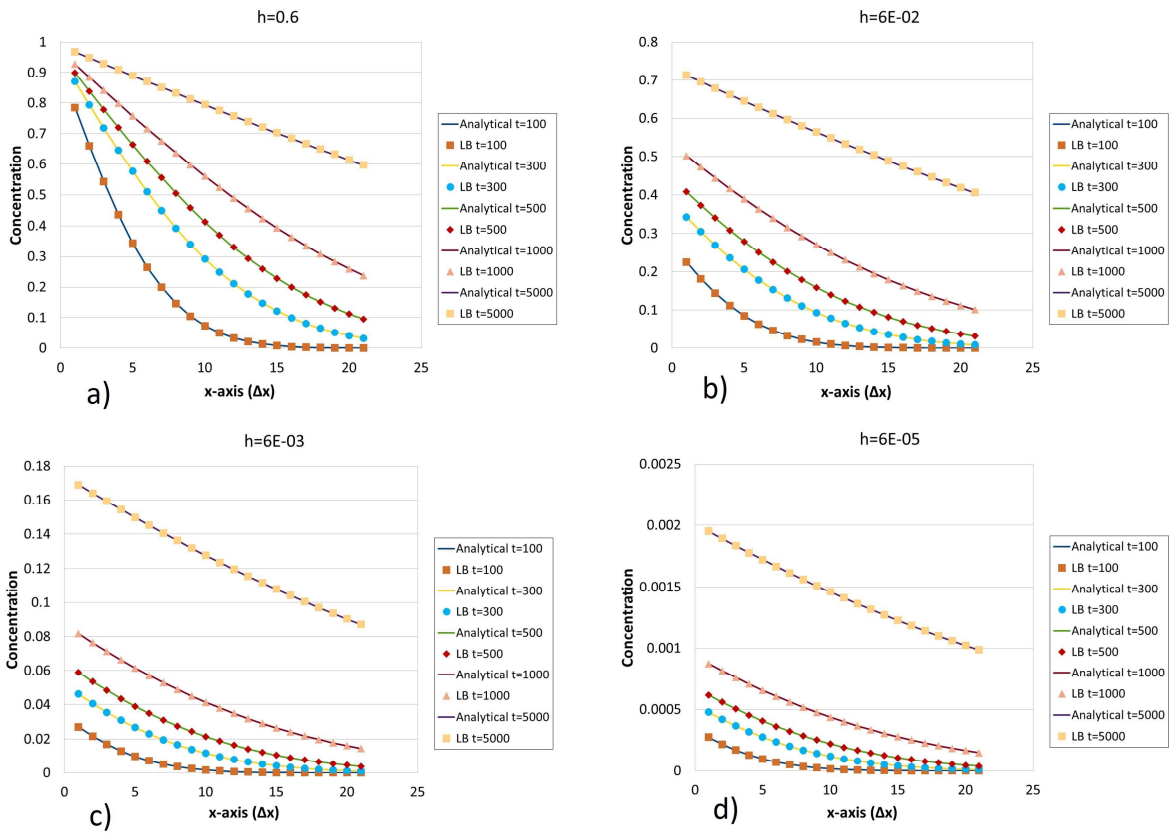

Fig. 3. Analytical solution (solid lines) and LB solution (markers) for reaction at a static interface for different times with different $h = \frac{k_R}{D}$. In all cases, C_{eq}=1 and C_o=0.

2. Curved static interface

The second test is performed to evaluate the model for a reaction imposed on a curved interface. We use the analytical solution for a cylinder with surface evaporation published in Crank [48]. We set an infinite cylinder with a diameter of 45 nodes in the middle of a 100x100 domain, as shown in Fig. 4. The surface of the cylinder (here in 2-D) at r=22.5 is subjected to a linear evaporation (reactive sink). We compare the truncated analytical solution (Eq. 23) for the concentration profile in the cylinder (first 6 terms of the analytical solution) with our numerical results at early time in Fig. 4 (a-c) for different reaction rates.

$$\frac{C-C_{in}}{C_{eq}-C_{in}} = 1 - \sum_{n=1}^{\infty} \frac{2 \cdot Da \cdot J_0\left(\frac{r\beta_n}{a}\right)}{(\beta_n^2 + Da^2) J_0(\beta_n)} \exp\left(-\frac{\beta_n^2 Dt}{a^2}\right) \qquad (23)$$

The β_n are the roots of:

$$\beta J_1(\beta) - Da J_0(\beta) = 0 \qquad (24)$$

J_i are the zero and first-order Bessel function and roots of Eq. (24) are given in [48] for several values of Da. C_{in}=0 is the initial concentration outside the cylinder and $r>a>0$ is the position where the analytical solution is calculated.

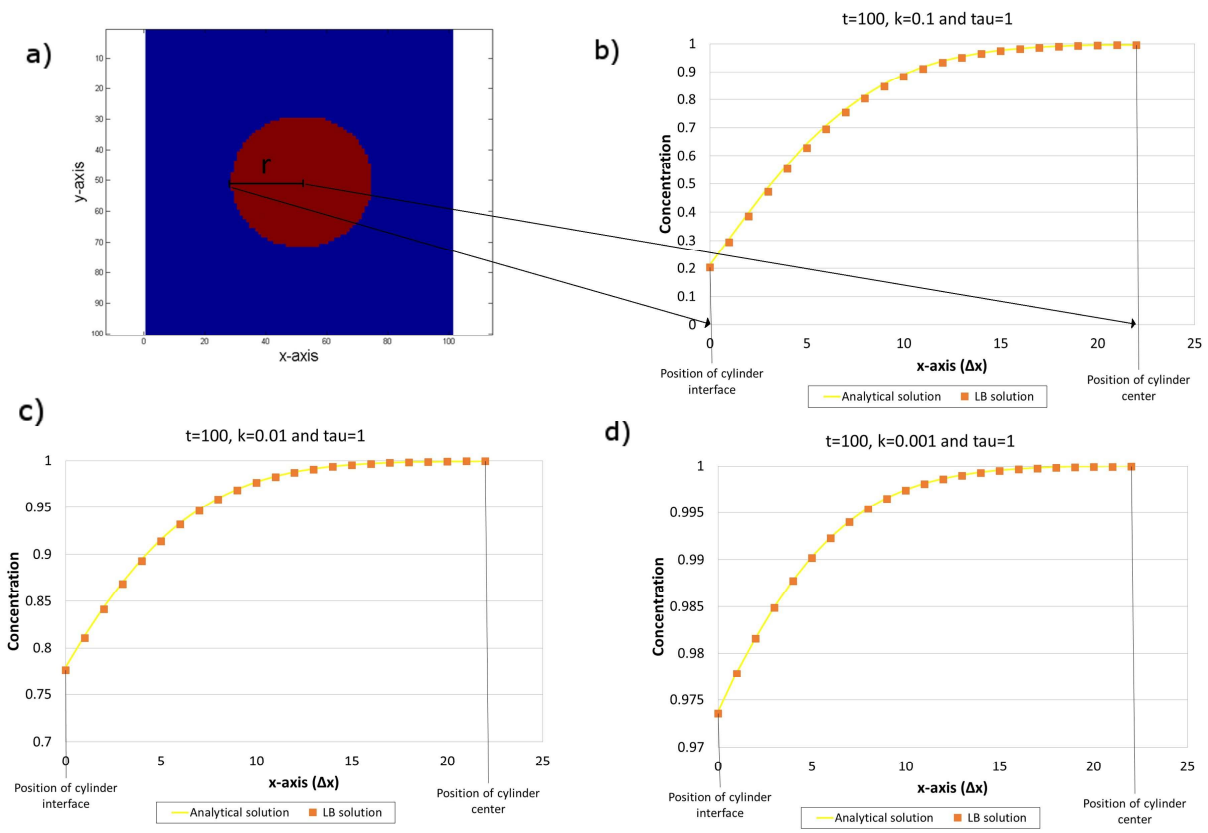

Fig. 4. Illustration of a cylinder in 2-D subjected to surface evaporation (a). Analytical solution (solid lines) and LB solution (markers) with evaporation at the surface of a cylinder at t=100 with k_r=0.1 (b), 0.01 (c), 0.001(d) and D=0.1667. In all cases, C_{eq}=1 and C_o=0.

Fig. 4 (b-d) shows a good agreement between the analytical and LB solution at early times. It is important to note that our model behaves well even if we use a staircase approximation of the interface. The magnitude of the first order staircase approximation should provide less accurate results when the curvature of the isocontours of concentration next to the cylinder surface is the highest, i.e. at early times.

3. Moving interface

The final test is aimed at testing our model with reactions taking place at a moving interface ($\mathbf{u}\neq 0$). Specifically, we show that the phase field method does not require an explicit treatment to correct Φ_R for the advective flux. In this model, the algorithm that imposes the reactive flux remains the same as for pure diffusion, which sets it apart from recent studies [28-29, 33]. In this test, the initial position of the interface is set at $\boldsymbol{x_{L/2}} = \boldsymbol{x_0}$, then $\varepsilon(\boldsymbol{x} \leq \boldsymbol{x_0}, t = 0) = 1$ and $\varepsilon(\boldsymbol{x} > \boldsymbol{x_0}, t = 0) = 0$. The phase field variable is updated during the simulation so that $\varepsilon(\boldsymbol{x} \leq \boldsymbol{x_0} + \boldsymbol{u}t, t) = 1$ and $\varepsilon(\boldsymbol{x} > \boldsymbol{x_0} + \boldsymbol{u}t, t) = 0$.

The analytical solution used is the same as in Eq. (15), where a change in reference frame is used to shift the position $\mathbf{x'}=\mathbf{x}+\mathbf{u}t$ as function of time. Fig. 5 (a-c) compares the concentration predicted by the numerical simulations with the corresponding analytical solution for different values of reaction rate with $\mathbf{u}$=0.01 l.u./t.s.. In Fig. 5 (d-f), we test our model over different diffusion coefficient values to vary the ratio of advective to diffusive transport, (i.e. the Peclet number). We observe that the numerical results agree very well with the analytical solution with no adjustment required for advective fluxes. No plots are shown for velocities $\mathbf{u}_w$<0.01, but we report that the agreement between the two solutions improves as the velocity decreases.

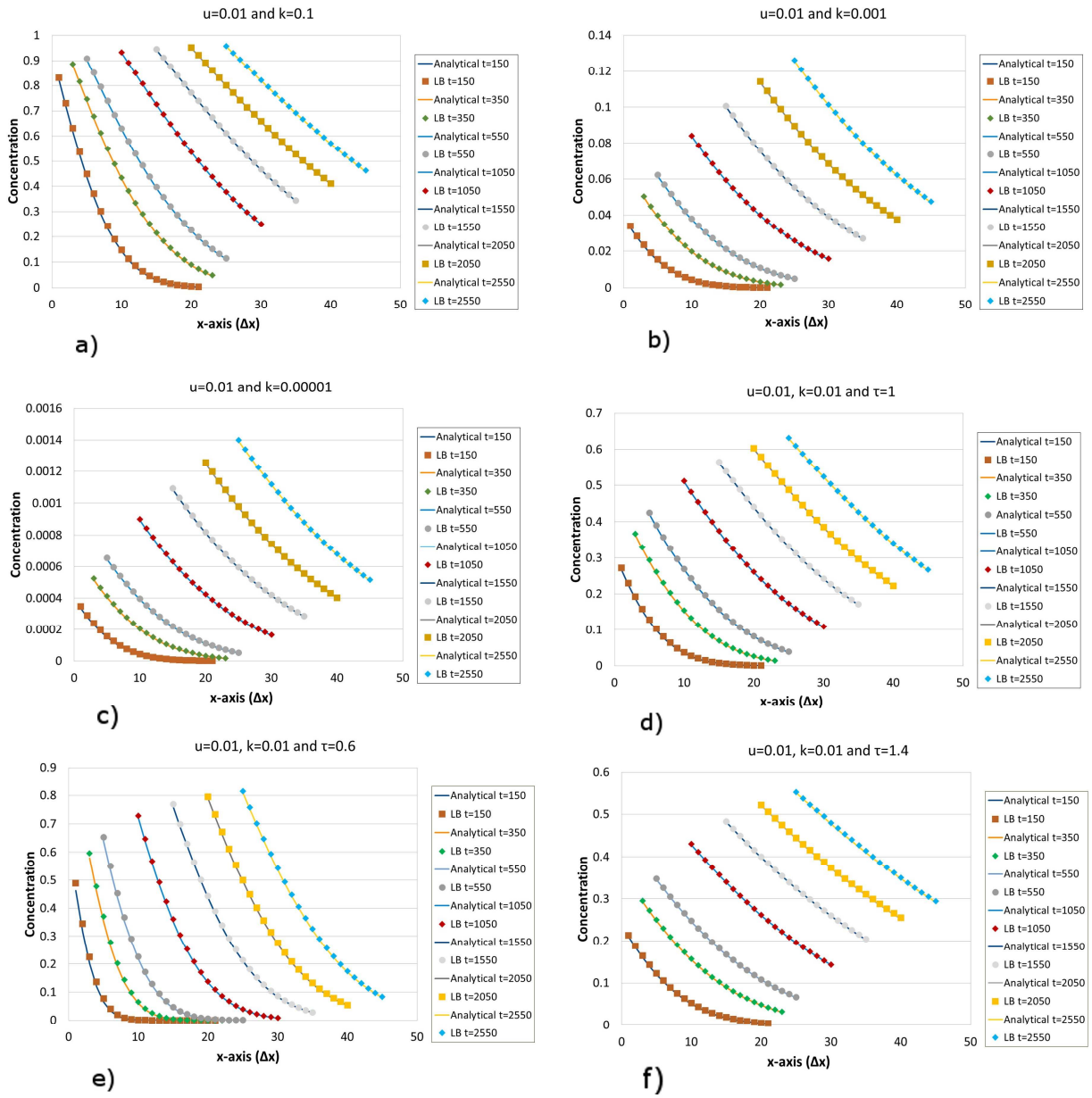

Fig. 5. (a-c) Analytical solution (solid lines) and LB solution (markers) for a moving interface at different times with D=1/6 and k_r=0.1(a), 0.001(b), 0.00001(c). (d-f) Analytical solution (solid lines) and LB solution (markers) for moving interface at different times for a fixed k_r=0.01 and

D=0.1667 (c), 0.0333 (d), 0.3 (f). The position of the interface from the starting point is shifted by x'=x+**u**t for the analytical solution. In all cases, C_{eq}=1 and C_o=0.

To examine the accuracy of the LB reactive scheme we evaluate the difference between numerical results and the analytical solution over a range of transport and reaction conditions (Peclet and Damkholer numbers). We quantify the quality of the fit by computing the (L_2) norm of the error in concentration across the domain with respect to the Peclet number (Pe):

$$Pe = \frac{uL}{D} \qquad (18)$$

which represents the ratio between advection and diffusion transport, where **u** is the flow discharge (velocity), L is a characteristic lengthscale and D is the diffusion coefficient. We also vary the Damkholer number:

$$Da = \frac{kL}{D} \qquad (19)$$

that characterizes the ratio of diffusive transport to reaction time scales.

Finally we define the mass Fourier number as:

$$Fo = \frac{Dt}{L^2} \qquad (20)$$

which allows us to normalize timescales with respect to diffusion. The time t corresponds to the time of the simulation and we select the characteristic length to be the grid spacing in the lattice (Δx=1 lattice units), in the absence of a clear characteristic lengthscale in the problem setup (semi-infinite media). We ran two simulations with *Fo*=33 and *Fo*=166 for a fixed reactive boundary and a single run time *Fo*= 51 for the moving boundary case, respectively, to study the effect of the temporal resolution on the accuracy of our model. In the case of static interface, we ran 54 simulations for each Fourier number (*Fo*=33 and *Fo*=166) changing *Da* and diffusivity (varying relaxation time). For each combination of *Da* and τ we compute the relative error and the mean squared error between the analytical and numerical solution defined as follows:

$$E_R = \frac{\sum_x |C_{analytical}(\mathbf{x},t) - C_{numerical}(\mathbf{x},t)|}{\sum_x |C_{analytical}(\mathbf{x},t)|} \qquad (21)$$

$$MSE = \frac{\sum_x \left(C_{analytical}(\mathbf{x},t) - C_{numerical}(\mathbf{x},t)\right)^2}{N_x} \qquad (22)$$

Where N_x represent the number of points where the difference between the two solutions solution is calculated. The logarithm of the MSE is plotted in Fig. 6 (a, b).

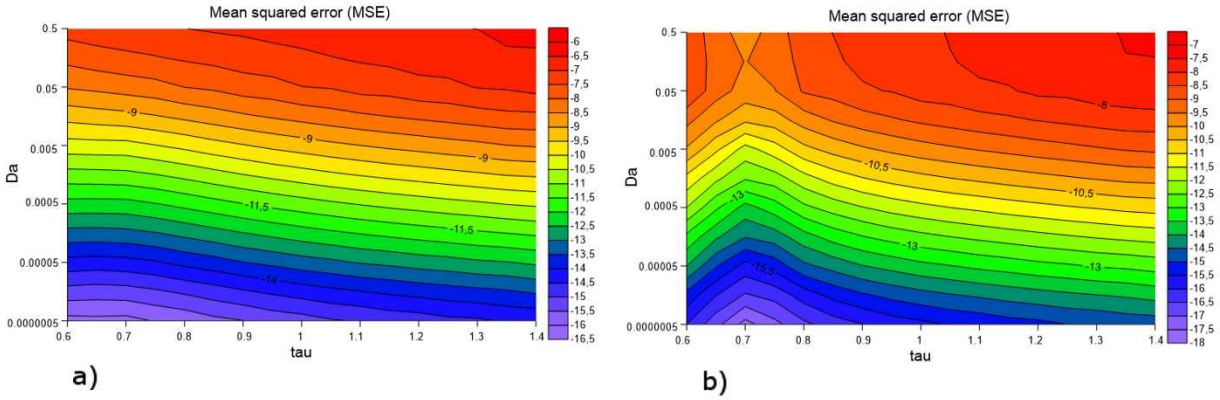

Fig. 6. (a) The distribution of Log(MSE) with *Fo*=33 for different *Da* numbers and relaxation times. (b) The distribution of Log(MSE) with *Fo*=166 for different *Da* numbers and relaxation times.

Results of relative error, not reported in this work, highlight as the time progresses (increasing *Fo*), the accuracy between the analytical and numerical solution increases by up to one order of magnitude in most simulations. Fig. 6(a-b) shows that the error decreases when the transport is set with low diffusion coefficient (smaller relaxation time). The LB model first loses accuracy and becomes unstable at very low or high relaxation time and for reaction rate $k_r > 0.5$, as reported also by Walsh and Saar [28]. This is probably due to the explicit nature of the transport scheme.

For the moving interface, we set the duration of each calculation to *Fo*=51 and run 18 simulations for 3 value of *Pe* number (*Pe*=0.5; 0.05; 0.005) and 6 choices of *Da* number. The choice of *Pe*<1 was motivated by the stability analysis of the ADE scheme by Suga [47], who pointed out that the D2Q5 scheme for solute transport is stable and more accurate for *Pe*<10. For larger *Pe* the solution could present oscillations. Table 1 and Fig. 7 show the results from these 18 simulations.

Da \ *Pe*	0.5	0.05	0.005
0.00002	2.40E-02	3.22E-02	2.55E-02
0.0002	2.40E-02	3.21E-02	2.55E-02
0.002	2.39E-02	3.20E-02	2.54E-02
0.02	2.32E-02	3.10E-02	2.47E-02
0.2	1.89E-02	2.54E-02	2.10E-02
2	1.47E-02	2.00E-02	1.78E-02

Table 1. Relative errors between the analytical and numerical solution for different relaxation times and *Da* numbers for moving interface with *Fo*=51.

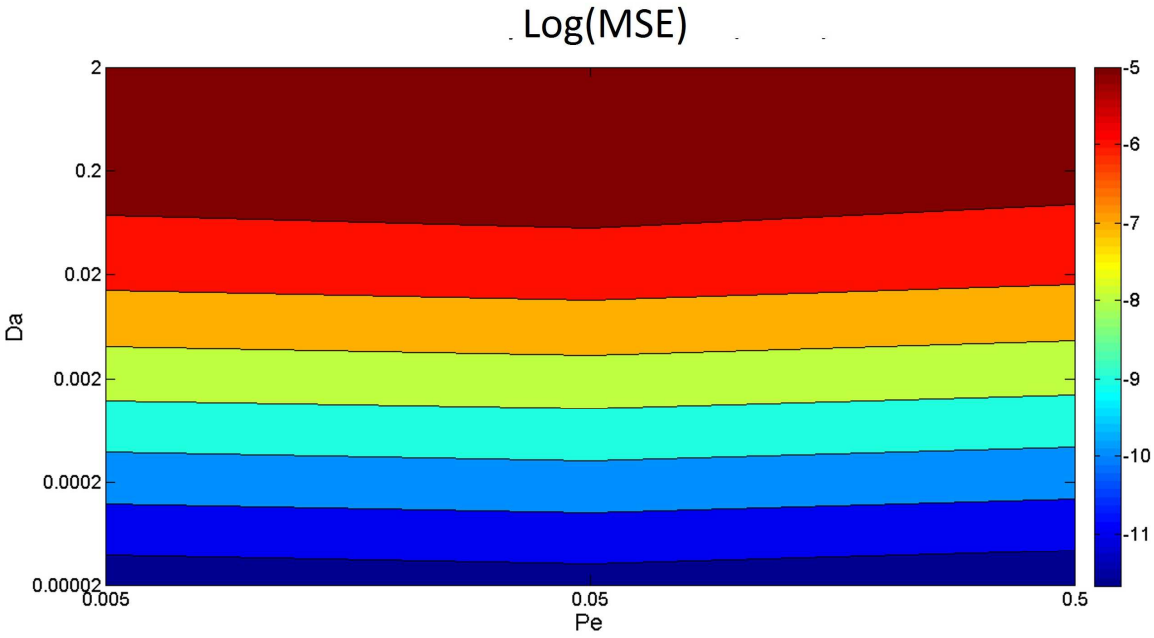

Fig. 7. The distribution of Log(MSE) in case of moving interface and *Fo*=51 with different Peclet numbers and Damkohler numbers.

In the case of a moving reactive interface, we observe that our model builds up most of the error when the interface position shifts to a neighbor site. This effect is due to the discrete way we update the interface position in the numerical model (the interface position is at all times located at the position of a node and only moved when $|\mathbf{u}\Delta t| + \mathbf{x} \geq \mathbf{x} + 1$. In Fig. 7, we show the logarithmic distribution of the MSE over a range of transport conditions (*Pe*) for several reaction rates (*Da*).

As seen from Fig. 7, the error decreases for slower reaction rates (lower *Da*). Additionally, we observe that *Pe* does only play a secondary role on the error, showing that the accuracy of our model is affected by *Da* but is independent of the transport regime for *Pe*<1.

IV. Multiphase dissolution simulation

Multiphase transport phenomena are of great interest in environmental sciences because many contaminated sites contain non-aqueous phase liquids (NAPLs). NAPLs are hazardous organic liquids that are immiscible with water. NAPL components can dissolve in water in very small amounts and at very low rates, acting as a long-term contamination source for groundwater. Therefore, it is difficult to design effective remediation schemes, partly due to hydrogeological factors, such as complex heterogeneities and the presence of low permeability zones. Dissolution of NAPLs occurs at the interface between water and the organic compound.

This final simulation aims to couple our LB reactive model with a multiphase flow and compute the mass transfer across the interface by dissolution of a fluid into another immiscible fluid. LB models for multiphase fluids range from the free-energy model of Swift et al [49], the color gradient model of Gunstensen [50] and the model of Shan and Chen ("SC") [51]. We chose the SC model because it has been used successfully in modeling different multiphase processes, such as capillary rise,

multiphase fluid flow in porous media, fingering phenomena, wetting properties and dissolution of immiscible fluids [27, 52-57, 61], even though the SC model is limited to small viscosity and density contrasts between the fluids [19, 22]. Recent studies have been developed to get over these limitations, by using realistic equation of state into the model and by increasing the isotropy of the interaction force [56-58].

We use one distribution function to solve for the momentum conservation for each of the two fluids. The LBM equation is written for each phase as:

$$f_i^k(\mathbf{x} + \boldsymbol{e_i}, t+1) = f_i^k(\mathbf{x}, t) + \Omega_i^k \qquad (25)$$

Where k denotes either fluid (1 or 2) and Ω_i^k is the collision operator which is simplified to a single relaxation time towards a local equilibrium (similar to Eq. (2)). The equilibrium functions are calculated with

$$f_i^{k,eq}(\mathbf{x}, t) = \omega_i \rho_k \left[1 + 3\frac{e_i \cdot u_k^{eq}}{c_s^2} + \frac{9}{2}\frac{\left(e_i \cdot u_k^{eq}\right)^2}{c_s^4} + \frac{3}{2}\frac{(u_k^{eq})^2}{c_s^4}\right] \qquad (26)$$

and the density for each fluid is obtained from $\rho_k = \sum_i f_i^k$. The macroscopic velocity $\mathbf{u}_k^{eq}$ is given by:

$$\boldsymbol{u}_k^{eq} = \boldsymbol{u}' + \frac{\tau_k \boldsymbol{F}_k}{\rho_k} \qquad (27)$$

Where $\boldsymbol{u}'$ is a composite velocity common to the two fluid components:

$$\mathbf{u}' = \frac{\sum_k \left(\sum_i \frac{f_i^k \cdot \mathbf{e}_i}{\tau_k}\right)}{\left(\sum_k \frac{\rho_k}{\tau_k}\right)}. \qquad (28)$$

In Eq. (27) the force term $\boldsymbol{F_k}$ acts on the kth component and includes adhesion (fluid-solid interaction) and cohesion forces (fluid-fluid interaction) between the two fluids. In the SC model the interaction force exerted by fluid $\bar{k}$ on fluid k is defined as:

$$\mathbf{F}_k(\boldsymbol{x}) = -\boldsymbol{G}_c \rho_k \sum_i w_i \rho_{\bar{k}}\,(x + \mathbf{e}_i \Delta t, t)\mathbf{e}_i\,. \qquad (29)$$

The magnitude of $\boldsymbol{G}_c$ controls the value of the surface tension σ with the Equation of State (EOS):

$$P = \frac{(\rho_k + \rho_{\bar{k}})}{3} + \boldsymbol{G}_c \frac{(\rho_k \cdot \rho_{\bar{k}})}{3}. \qquad (30)$$

We set a simulation inspired from that proposed by Chen and Zhang [27] and later repeated by Walsh and Saar [28]. The simulation we propose differs because we consider a collection of droplets with different sizes. The simulation domain consist of 400 and 600 nodes perpendicular and parallel to gravity respectively. The left and right boundaries are set as no-slip walls while the bottom and top of the domain are set as periodic boundary conditions. Eleven immiscible droplets are initially randomly distributed at the bottom of the domain, as shown in Fig. 8(a).

In order to characterize the system, we introduce the Bond number *Bo,* defined as the ratio of buoyancy forces to surface tension

$$Bo = \frac{(\rho_1 - \rho_2) g d^2}{\sigma}, \qquad (32)$$

where g is the gravitational acceleration, ρ_1 and ρ_2 are the densities of fluid 1 and fluid 2 and d is the droplet diameter (here we use the largest droplet as a reference). The interfacial tension σ between the two fluids was calibrated with Eq. (30) under equilibrium conditions (Laplace-Young's law), and yielded $\sigma \approx 0.08$. The SC model does not allow significant density contrasts between the immiscible fluids. We introduce a bulk force in the collision for the discrete fluid (droplet) which we will use as a simple proxy to generate the buoyancy force for the droplets.

We set the kinematic viscosity of both fluids to be identical (ν=1/6 lattice units) and the buoyancy force per unit volume for the droplets is set to 0.0001 and it is directed upward in the vertical direction. The reaction rate constant at the interface between the fluids is fixed to 0.01. These parameters yield $Bo \approx 1$ (defining the characteristic lengthscale as the size of the largest droplets) and $Da \approx 2$. The Bond number value was selected to display some small deformation for the largest droplets. The simulation time is normalized with $t_c = \frac{L^2}{D}$.

The diffuse interface between the immiscible fluids that emerges from the SC model allows for different interpretation for the position of the interface. Sukop and Thorne [21] provide three methods to evaluate the boundary surface, each of these shows a different accuracy in reproducing Laplace's law. For these calculations, we identify the location of the reactive interface between the two immiscible fluids with the location where the droplet density becomes greater than the density of the other fluid. This criterion results easy to implement and gives good agreement with Laplace's equation [28].

As assumed in [26], the dissolution rate is much lower than the decrease of droplet radius and we therefore neglect droplet volume reduction by mass loss. The results of the simulations are shown in Fig. 8. The droplets start to move upward because they are positively buoyant and their rise velocity increases until they reach a steady state migration velocity. The dissolution starts at the beginning of the simulation even if the flow field around the droplets is not fully developed.

At the first steps of the simulation, the solute transport is controlled by diffusion, as observed in Fig. 8(a) with the isotropic concentration around the droplets. When the velocity of droplets approaches steady-state (Fig. 8(b-e)) the advective transport becomes predominant and the dissolved mass of suspended fluid is mostly distributed along the tail of the ascending droplets. We observe coalescence during the motion of droplets. Although the range of dimensionless numbers used here are similar to those of Walsh and Saar [28] and Chen and Zhang [27], our calculations do not generate significant fictitious lobes of high concentration at the top, bottom, and sides of the bubble as observed in [27]. The main difference between our simulation and that of Chen and Zhang [27] is that the droplets are more buoyant in our case, i.e. much higher Bond number, and consequently faster ascent velocity. Moreover, the rate of solute diffusion is also known to influence the accumulation of error caused by spurious currents during multiphase solute transport [61]. Parmigiani [61] highlighted that the error between a multi-component model (in that particular case he used a Shan Chen multiphase model together with an advection-diffusion equation for heat transport) can be less than 2% for a choice of advection-diffusion relaxation time greater than 0.55. In our calculations, the rising velocity of the droplets is high enough that the relative error associated with spurious current is less apparent but still present and the relaxation time for the solute transport model is set to 0.6. Walsh and Saar eliminated this issue by using an immiscible model with reduced interface velocities. Also Chen et al. [33] solved the problem adopting the Carnahan-Starling EOS, which generates small spurious currents.

This simulation aims to highlight the ability of our LB reactive model handles complex time-dependent geometries. We want to point out the simplicity of the algorithm and the ease of implementation, which uses the phase field method to calculate/identify the normal direction of the flux, while the concentration at the interface is calculated by an iterative scheme avoiding finite difference discretization or half-way bounce-back. The reactive scheme is introduced into the classical LB algorithm and is applied just where an interface is identified with the phase-field, but the treatment is independent of interface orientation and velocity.

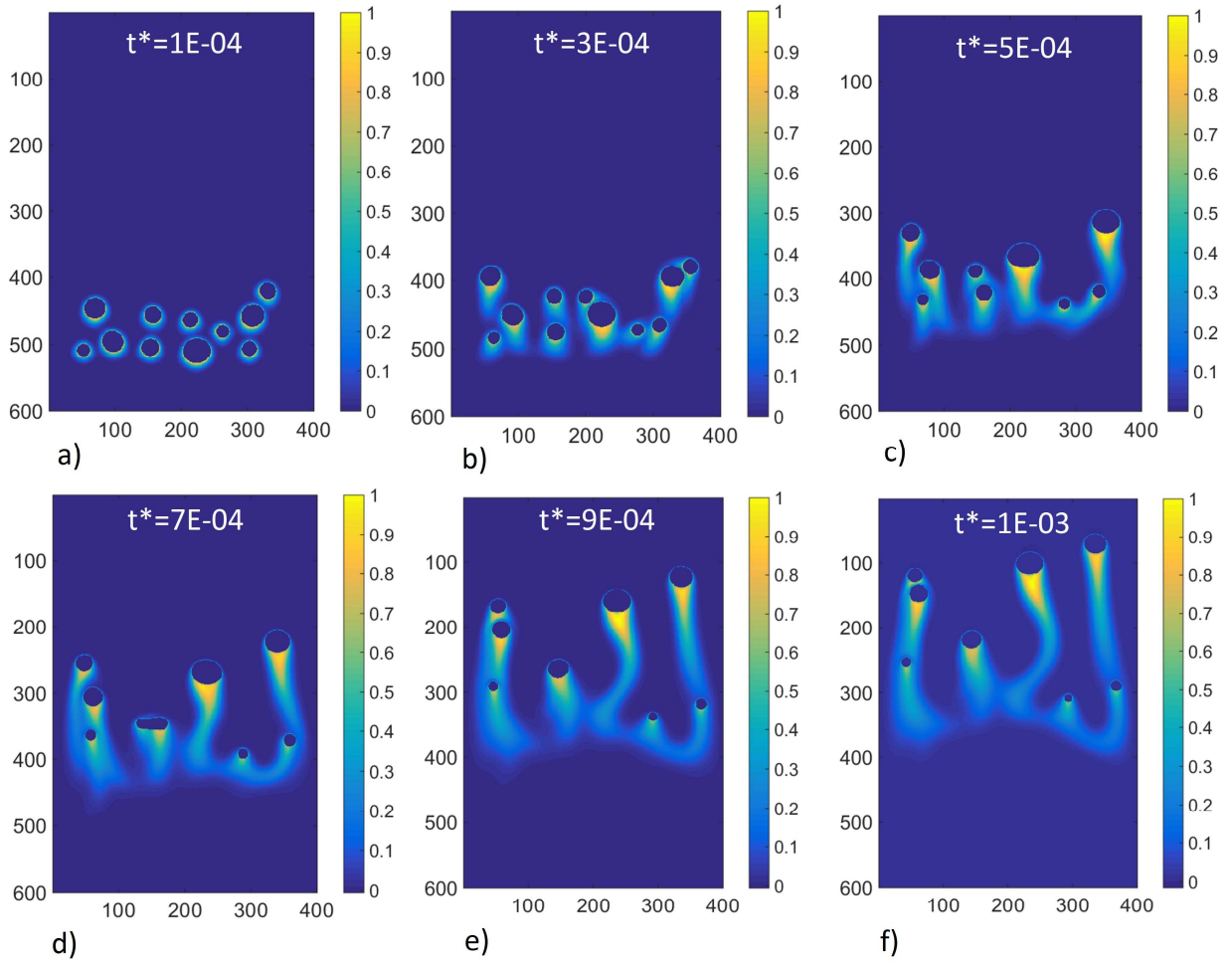

Fig. 8. Snapshots of rising droplets dissolving due to interface reaction. The concentration inside the droplets is normalized (C_{eq}=1) and time is normalized by the characteristic time $t_c = \frac{L^2}{D}$.

V. Conclusions

In this work, we propose a new lattice Boltzmann scheme to simulate interface reactions between immiscible fluids. The model is based on the phase-field method and the sites where the heterogeneous reactions occur follow a similar evolution rule as the bulk of each fluid phase. This offers the advantage that the treatment of interface reactions becomes independent of the topology and orientation of the interface. The model has been validated with different benchmark examples

and in all simulations, the agreement between the numerical and analytical solution is found to be excellent. We also present tests for curved and moving interfaces. We found that the accuracy of our model increases with the progress of simulations and that the transport regime exerts only a secondary role on the accuracy of the scheme, while the model is more accurate at low *Da*. In the last test, we couple our model to a two-phase Shan Chen LB model and simulate the mass transfer by dissolution in a droplet suspension.

In the future, we argue that a natural extension of this model is to apply this multiphase reactive transport in porous media to consider realistic remediation scenarios. Further extending the model to multicomponent chemical reactive transport, following the models of Kang [26], Chen [33] and Huber [35] will offer the possibility to improve the description of the physico-chemical and biological processes that control the mass balance of pollutant at the pore-scale.

Acknowledgements

The Authors would like to thank you the Water Research Institute (IRSA) of Italian National Council (CNR) for the financial support. In addition, we thank Elisa Martorelli for supporting the multiphase simulation and Andrea Parmigiani for helpful discussions. Christian Huber acknowledges support from NSF EAR 1144957.

VI. References

[1] Mayer A, Hassanizadeh S. Soil and groundwater contamination: Nonaqueous phase liquids. American Geophysical Union; 2005. http://dx.doi.org/10.1029/WM017.

[2] Bear J. Dynamics of fluids in porous media. Courier Dover Publication, 2013. http://dx.doi.org/10.1017/S0022112073210662.

[3] Fetter C. Applied hydrogeology. Upper Saddle River, NJ: Prentice Hall, 2001.

[4] Bedient P, Rifai H, Newell C. Ground water contamination: transport and remediation. Prentice-Hall International, Inc., 1994.

[5] Thullner M, Mauclaire L, Schroth M, Kinzelbach W, Zeyer, J. Interaction between water flow and spatial distribution of microbial growth in a two-dimensional flow field in saturated porous media. Journal of Contaminant Hydrology 2002; 58(3): pp 169-189. http://dx.doi.org/10.1016/S0169-7722(02)00033-5.

[6] Knutson C, Werth C, Valocchi A. Pore-scale simulation of biomass growth along the transverse mixing zone of a model two-dimensional porous medium. Water resources research 2005; 41(7) http://dx.doi.org/10.1029/2004WR003459.

[7] Abriola L. Modeling multiphase migration of organic chemicals in groundwater systems. A review and assessment. Environmental Health Perspectives 1989; 83: 117–143.

[8] Rivett M, Feenstra S, Cherry J. Transport of a dissolved phase plume from a residual solvent source in a sand aquifer. Journal of Hydrology 1994; 159 (1–4): 27–41.

[9] Lee K, Chrysikopoulos C. Numerical modeling of three-dimensional contaminant migration from dissolution of multicomponent NAPL pools in saturated porous media. Environmental Geology 1995; 26 (3): 157–165.

[10] Parker J, Park E. Modeling field-scale dense non-aqueous phase liquid dissolution kinetics in heterogeneous aquifers. Water Resources Research 2004; 40(5): W051091–W0510912. http://dx.doi.org/10.1029/2003WR002807.

[11] Christ J, Abriola L. Modeling metabolic reductive dechlorination in dense non-aqueous phase liquid source-zones. Advances in water resources 2007; 30(6): 1547-1561. http://dx.doi.org/10.1016/j.advwatres.2006.05.024.

[12] Manoli G, Chambon J, Bjerg P, Scheutz C, Binning P, Broholm M. A remediation performance model for enhanced metabolic reductive dechlorination of chloroethenes in fractured clay till. Journal of contaminant hydrology 2012; 131(1): 64-78. http://dx.doi.org/10.1016/j.jconhyd.2012.01.004.

[13] McLaren R, Sudicky E, Park Y, Illman W. Numerical simulation of DNAPL emissions and remediation in a fractured dolomitic aquifer. Journal of Contaminant Hydrology 2012; 136-137: 56–71. http://dx.doi.org/10.1016/j.jconhyd.2012.05.002.

[14] Viotti P, Di Palma P, Aulenta F, Luciano A, Mancini G, Papini M. Use of a reactive transport model to describe reductive dechlorination (RD) as a remediation design tool: application at a CAH-contaminated site. Environmental Science and Pollution Research 2014; *21*(2): 1514-1527. http://dx.doi.org/10.1007/s11356-013-2035-9.

[15] Bear J, Verruijt A. Modeling groundwater flow and pollution. Vol. 2. Springer, 1987.

[16] Clement T, Johnson C, Sun Y, Klecka G, Bartlett C. Natural attenuation of chlorinated ethene compounds: Model development and field-scale application at the Dover site, J. Contam. Hydrol. 2002; 42: pp 113– 140. http://dx.doi.org/10.1016/S0169-7722(99)00098-4.

[17] Gramling C, Harvey C, Meigs L. Reactive transport in porous media: A comparison of model prediction with laboratory visualization. Environ. Sci. Technol. 2002; 36: 2508–2514. http://dx.doi.org/10.1021/es0157144.

[18] Qian Y, d'Humières D, Lallemand P. Lattice BGK models for Navier-Stokes equation. EPL (Europhysics Letters) 1992; *17*(6): 479. http://dx.doi.org/10.1209/0295-5075/17/6/001.

[19] Chen S, Doolen G. Lattice Boltzmann method for fluid flows. Annual review of fluid mechanics 1998; 30 (1): 329-364. http://dx.doi.org/10.1146/annurev.fluid.30.1.329.

[20] Succi S. The lattice Boltzmann equation for fluid dynamics and beyond. Oxford University Press, Oxford 2001. http://dx.doi.org/10.1016/S0997-7546(02)00005-5.

[21] Sukop M, Thorne D. Lattice Boltzmann Modeling 2006. Springer, Heidelberg.

[22] Aidun C, Clausen J. Lattice-Boltzmann method for complex flows. Annual Review of Fluid Mechanics 2010; 42: 439-472. http://dx.doi.org/10.1146/annurev-fluid-121108-145519.

[23] Huber C, Chopard B, Manga M. A lattice Boltzmann model for coupled diffusion. Journal of Computational Physics 2010; 229(20): 7956-7976.

[24] Kang Q, Zhang D, Chen S, He X. Lattice Boltzmann simulation of chemical dissolution in porous media. Physical Review E 2002; 65(3): 036318. http://dx.doi.org/10.1103/PhysRevE.65.036318.

[25] Kang Q, Lichtner PC, Zhang D. Lattice Boltzmann pore-scale model for multicomponent reactive transport in porous media. J Geophys Res Solid Earth 2006; 111: 1978–2012. http://dx.doi.org/10.1029/2005JB003951.

[26] Kang Q, Lichtner P, Zhang D. An improved lattice Boltzmann model for multicomponent reactive transport in porous media at the pore scale. Water Resources Research 2007; 43 (12). http://dx.doi.org/10.1029/2006WR005551.

[27] Chen C, Zhang D. Lattice Boltzmann simulation of the rise and dissolution of two-dimensional immiscible droplets. Physics of Fluids (1994-present) 2009; 21 (10): 103301. http://dx.doi.org/10.1063/1.3253385.

[28] Walsh S, Saar M. Interpolated lattice Boltzmann boundary conditions for surface reaction kinetics. Physical Review E 2010; 82(6): 066703. http://dx.doi.org/10.1103/PhysRevE.82.066703.

[29] Zhang T, Shi B, Guo Z, Chai Z, Lu J. General bounce-back scheme for concentration boundary condition in the lattice-Boltzmann method. Physical Review E 2012; 85(1): 016701. http://dx.doi.org/10.1103/PhysRevE.85.016701.

[30] Chen Q, Zhang X, Zhang J. Improved treatments for general boundary conditions in the lattice Boltzmann method for convection-diffusion and heat transfer processes. Physical Review E 2013; 88.3: 033304. http://dx.doi.org/10.1103/PhysRevE.88.033304.

[31] Gillissen J, Looije N. Boundary conditions for surface reactions in lattice Boltzmann simulations. Physical Review E 2014; *89*(6): 063307. http://dx.doi.org/10.1103/PhysRevE.89.063307.

[32] Ladd A. Numerical simulations of particulate suspensions via a discretized Boltzmann equation. Part 1. Theoretical foundation. Journal of Fluid Mechanics 1994; 271: 285-309. http://dx.doi.org/10.1017/S0022112094001771.

[33] Chen L, Kang Q, Robinson B, He Y, Tao W. Pore-scale modeling of multiphase reactive transport with phase transitions and dissolution-precipitation processes in closed systems. Physical Review E. 2013; 87(4): http://dx.doi.org/043306.10.1103/PhysRevE.87.043306.

[34] Huber C, Parmigiani A, Chopard B, Manga M, Bachmann O. Lattice Boltzmann model for melting with natural convection. International Journal of Heat and Fluid Flow 2008; *29*(5): 1469-1480. http://dx.doi.org/10.1016/j.ijheatfluidflow.2008.05.002.

[35] Huber C, Shafei B, Parmigiani A. A new pore-scale model for linear and non-linear heterogeneous dissolution and precipitation. Geochimica et Cosmochimica Acta 2014; 124: 109-130. http://dx.doi.org/10.1016/j.gca.2013.09.003.

[36] Dawson S, Chen S, Doolen D. Lattice Boltzmann computations for reaction-diffusion equations. The Journal of chemical physics 1993; 98(2): 1514-1523. http://dx.doi.org/10.1063/1.464316.

[37] Higuera F, Jimenez J. Boltzmann approach to lattice gas simulations. EPL (Europhysics Letters) 1989; *9*(7): 663. http://dx.doi.org/10.1209/0295-5075/9/7/009.

[38] Ginzburg I. (2005) Equilibrium-type and link-type lattice Boltzmann models for generic advection and anisotropic-dispersion equation. Advances in Water Resources 2005; 28: 1171–1195. http://dx.doi.org/10.1016/j.advwatres.2005.03.004.

[39] Stiebler M., Tölke J. Krafczyk M. (2008) Advection–diffusion lattice Boltzmann scheme for hierarchical grids. Comp. Math. Appl. 2008; 55: 1576–1584. http://dx.doi.org/10.1016/j.camwa.2007.08.024.

[40] Flekkøy E. Lattice Bhatnagar-Gross-Krook models for miscible fluids. Physical Review E 1993; 47: 4247. http://dx.doi.org/10.1103/PhysRevE.47.4247.

[41] Huang H, Lu X, Sukop M. Numerical study of lattice Boltzmann methods for a convection–diffusion equation coupled with Navier–Stokes equations. J. Phys. A: Math. Theor. 2011; 44**:** 055001. http://dx.doi.org/10.1088/1751-8113/44/5/055001.

[42] Peng Y, Zhou J, Burrows R. Modelling solute transport in shallow water with the lattice Boltzmann method. Computers & Fluids 2011; 50: 181–188. http://dx.doi.org/10.1016/j.compfluid.2011.07.008.

[43] Latt J. Hydrodynamic limit of lattice Boltzmann equations 2007. Thèse de doctorat: Univ. Genève. http://archive-ouverte.unige.ch/unige:464

[44] Chopard B, Falcone J, Latt J. The lattice Boltzmann advection-diffusion model revisited. The European Physical Journal-Special Topics 2009; *171*(1): 245-249.http://dx.doi.org/10.1140/epjst/e2009-01035-5.

[45] Zou, Q, He X. On pressure and velocity boundary conditions for the lattice Boltzmann BGK model. Physics of Fluids (1994-present) 1997; *9*(6): 1591-1598. http://dx.doi.org/10.1063/1.869307.

[46] Zhang X, Crawford J, Bengough G, Young, I. On boundary conditions in the lattice Boltzmann model for advection and anisotropic dispersion equation. Advances in water resources 2002; *25*(6): 601-609. http://dx.doi.org/10.1016/S0309-1708(02)00027-1.

[47] Suga K. Lattice Boltzmann methods for complex micro-flows: applicability and limitations for practical applications. Fluid Dyn. Res. 2013; 45: 034501. http://dx.doi.org/10.1088/0169-5983/45/3/034501.

[48] Crank J. The mathematics of diffusion. 1975; 2nd Edition Oxford Science Publications.

[49] Swift M, Osborn W, Yeomans J. Lattice Boltzmann simulation of nonideal fluids, Phys. Rev. Lett. 1995; 75 (5): 830–833. http://dx.doi.org/10.1103/PhysRevLett.75.830.

[50] Gunstensen K. Ph.D. thesis, MIT, 1992.

[51] Shan X, Chen H. Lattice Boltzmann model for simulating flows with multiple phases and components. Phys Rev E 1993; 47:3 http://dx.doi.org/10.1103/PhysRevE.47.1815.

[52] Knutson C, Werth C, Valocchi A. Pore-scale modeling of dissolution from variably distributed nonaqueous phase liquid blobs. Water Resources Research 2001; 37(12): 2951-2963. http://dx.doi.org/10.1029/2001WR000587.

[53] Kang Q, Zhang D, Chen S. Displacement of a two-dimensional immiscible droplet in a channel. Physics of Fluids (1994-present), 2002; 14(9): 3203-3214. http://dx.doi.org/10.1063/1.1499125.

[54] Pan C, Hilpert M, Miller C. Lattice-Boltzmann simulation of two-phase flow in porous media. Water Resour Res 2004; 40. http://dx.doi.org/10.1029/2003WR002120.

[55] Parmigiani A, Huber C, Bachmann O, Chopard B. Pore-scale mass and reactant transport in multiphase porous media flows. Journal of Fluid Mechanics 2011; *686*, 40. http://dx.doi.org/10.1017/jfm.2011.268.

[56] Chen L, Kang Q, Mu Y, He Y, Tao W. A critical review of the pseudopotential multiphase lattice Boltzmann model: Methods and applications. International Journal of Heat and Mass Transfer 2014; 76: 210-236. doi:10.1016/j.ijheatmasstransfer.2014.04.032.

[57] Yuan P, Schaefer L. Equations of state in a lattice Boltzmann model. Phys. Fluids 2006; 18 (4): 042101–042111. doi:10.1016/j.apm.2012.04.048.

[58] Bao J, Schaefer L. Lattice Boltzmann equation model for multi-component multi-phase flow with high density ratios. Applied Mathematical Modelling 2013; 37.4: 1860-1871. http://dx.doi.org/10.1063/1.2187070

[59] Huber C, Parmigiani A, Latt J, Dufek J. Channelization of buoyant nonwetting fluids in saturated porous media. Water Resources Research 2013; *49*(10): 6371-6380. http://dx.doi.org/10.1002/wrcr.20514.

[60] Huang H, Thorne Jr D, Schaap M, Sukop M. Proposed approximation for contact angles in Shan-and-Chen-type multicomponent multiphase lattice Boltzmann models. Physical Review E, 2007; 76(6): 066701. http://dx.doi.org/10.1103/PhysRevE.76.066701.

[61] Parmigiani A. Lattice Boltzmann calculations of reactive multiphase flows in porous media. Ph.D. thesis, University of Geneva, 2011.

Figure 1

a) D2Q9 Scheme

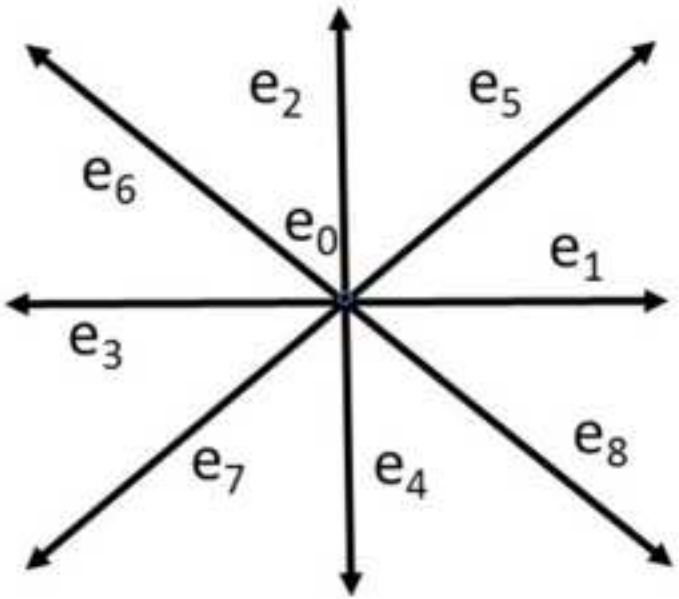

b) D2Q5 Scheme

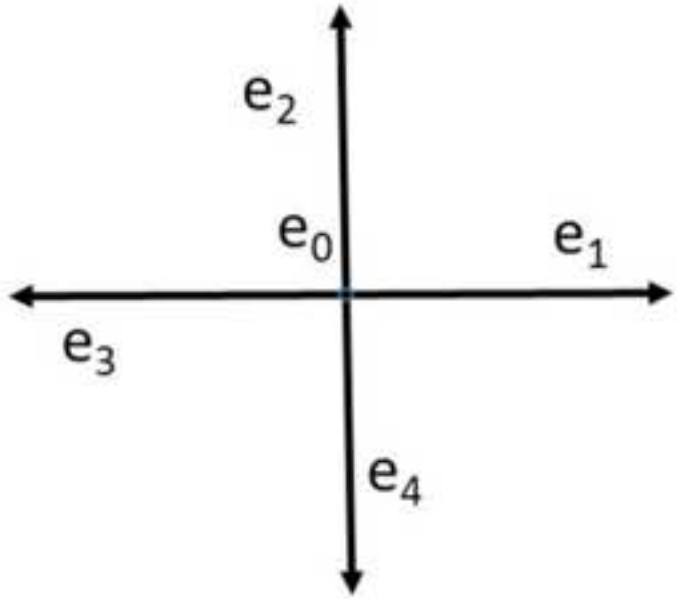

Figure 2

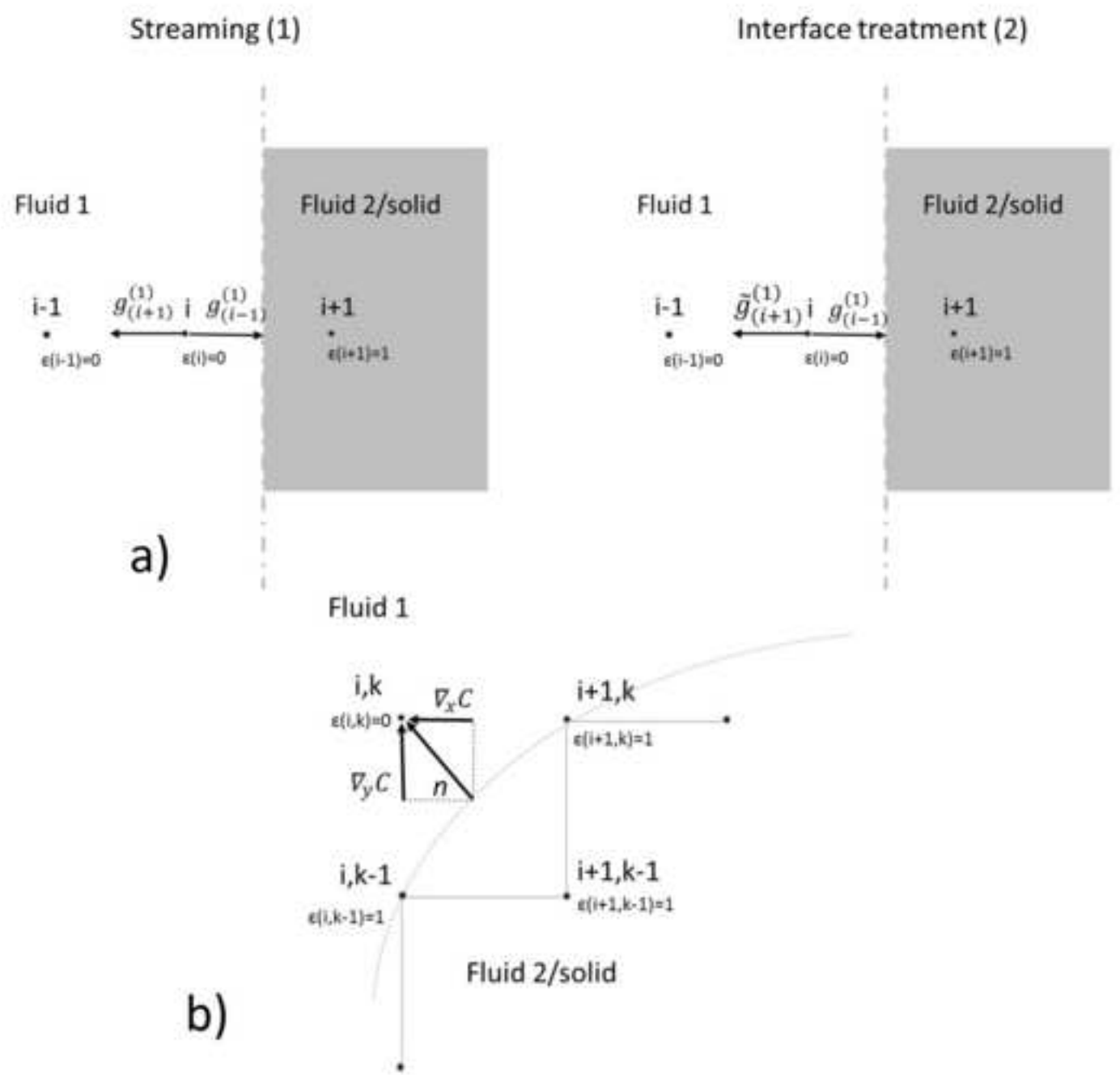

Figure 3

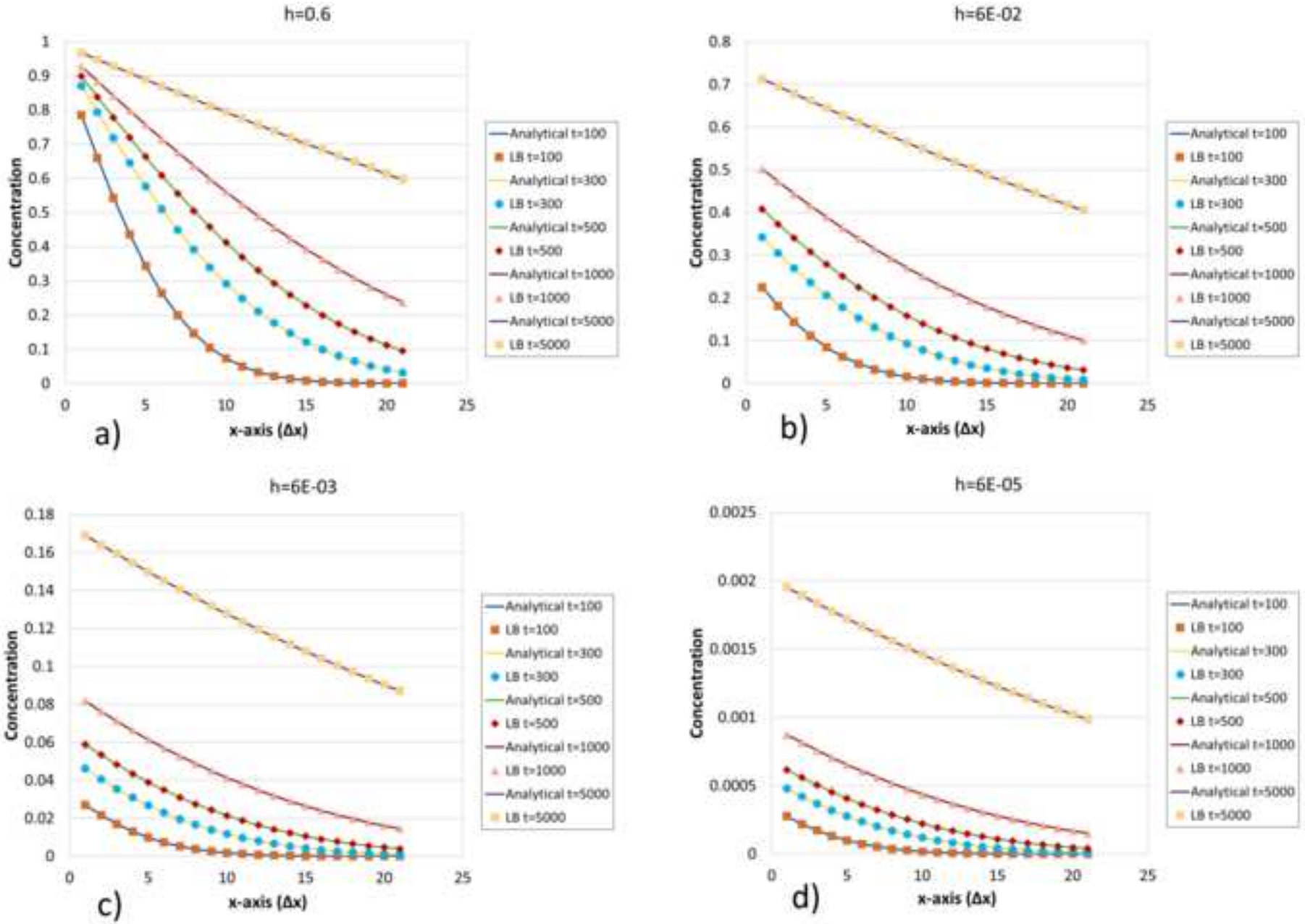

Figure 4

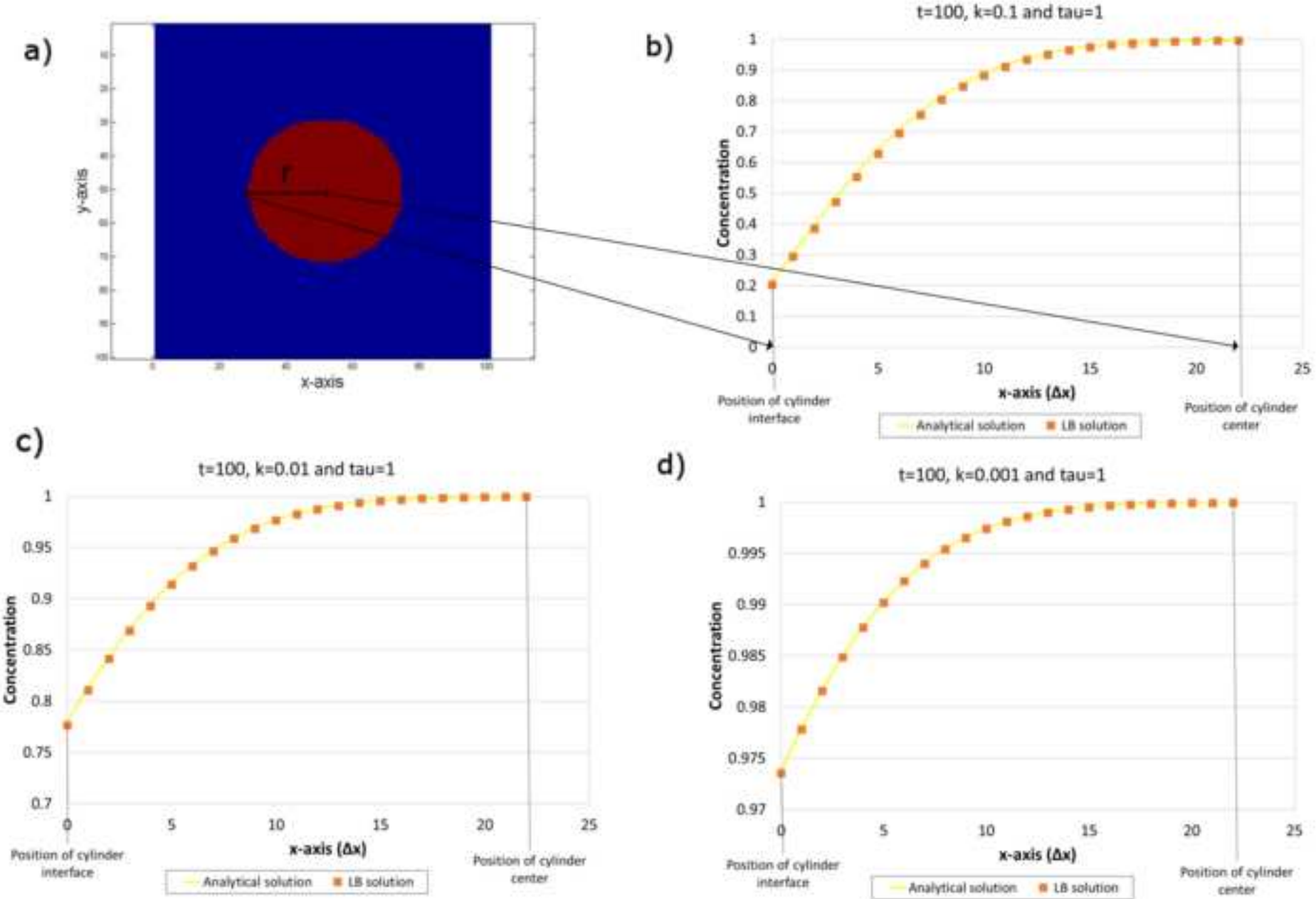

Figure 5

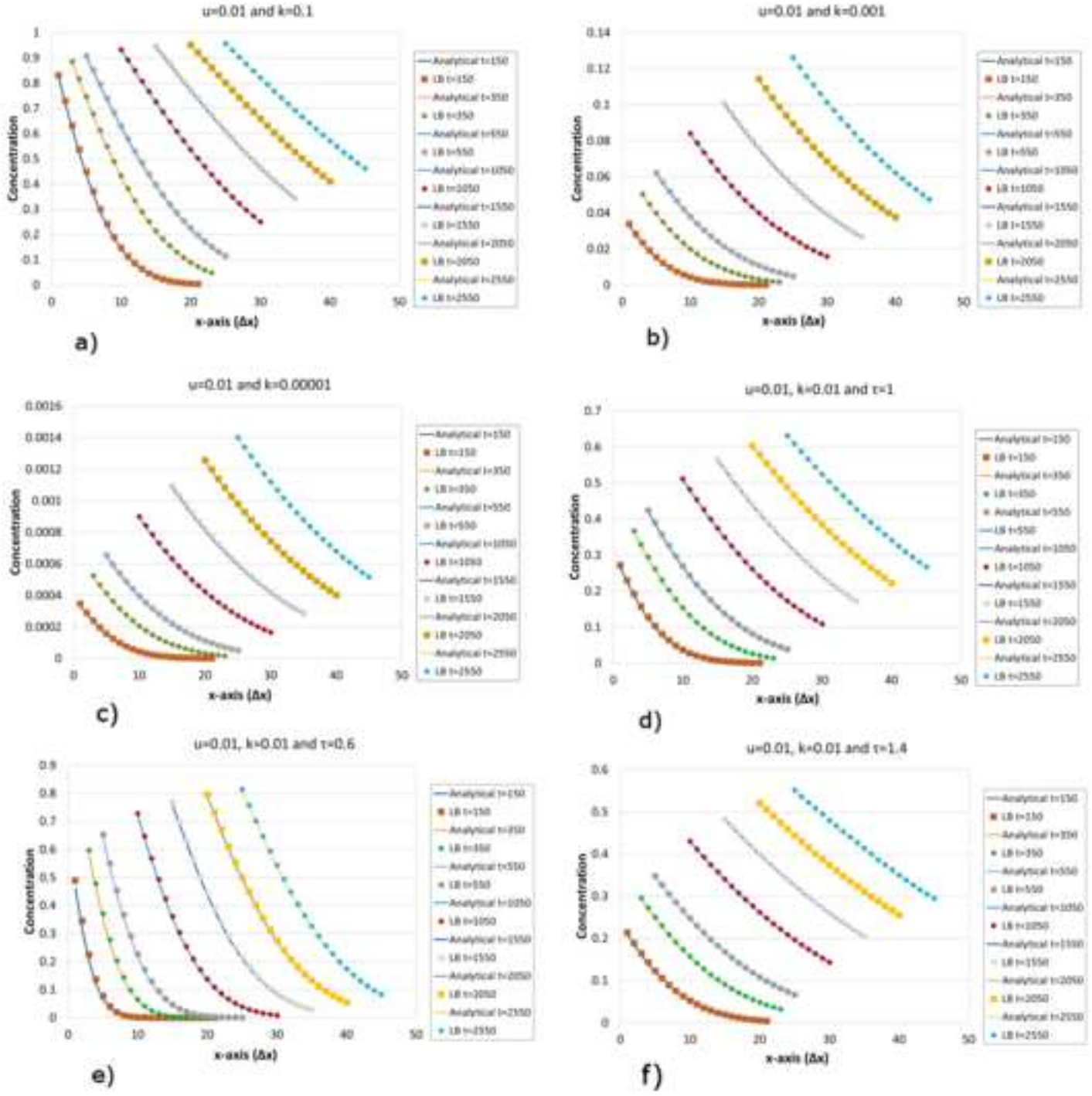

Figure 6

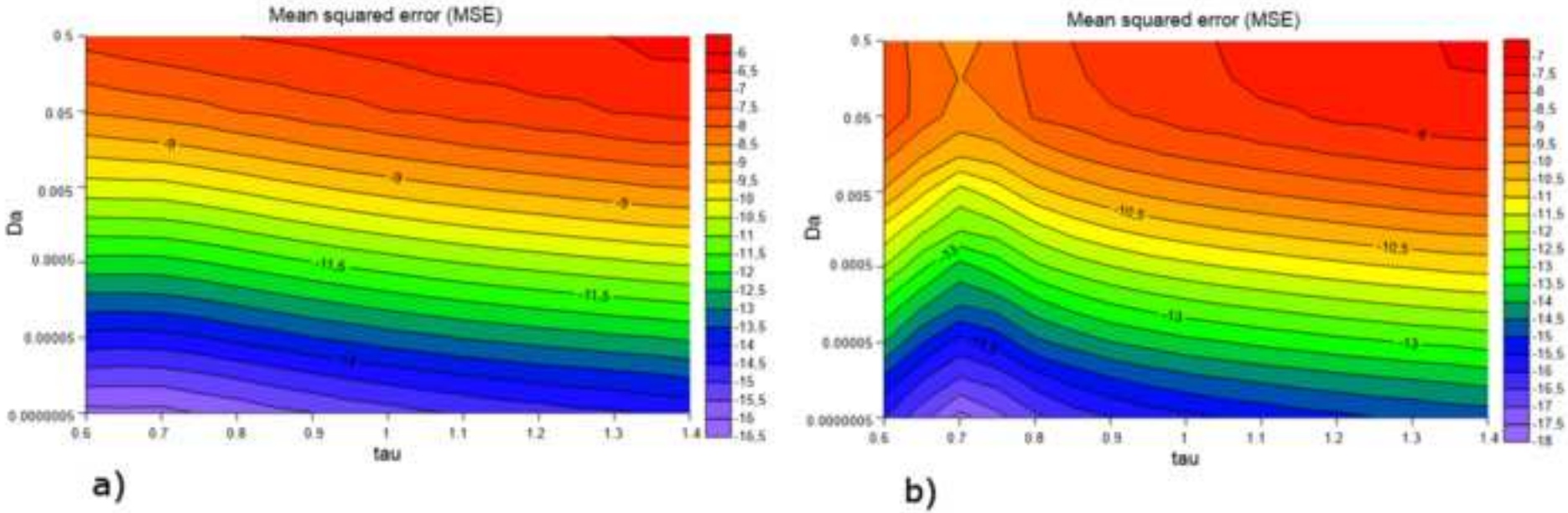

Figure 7

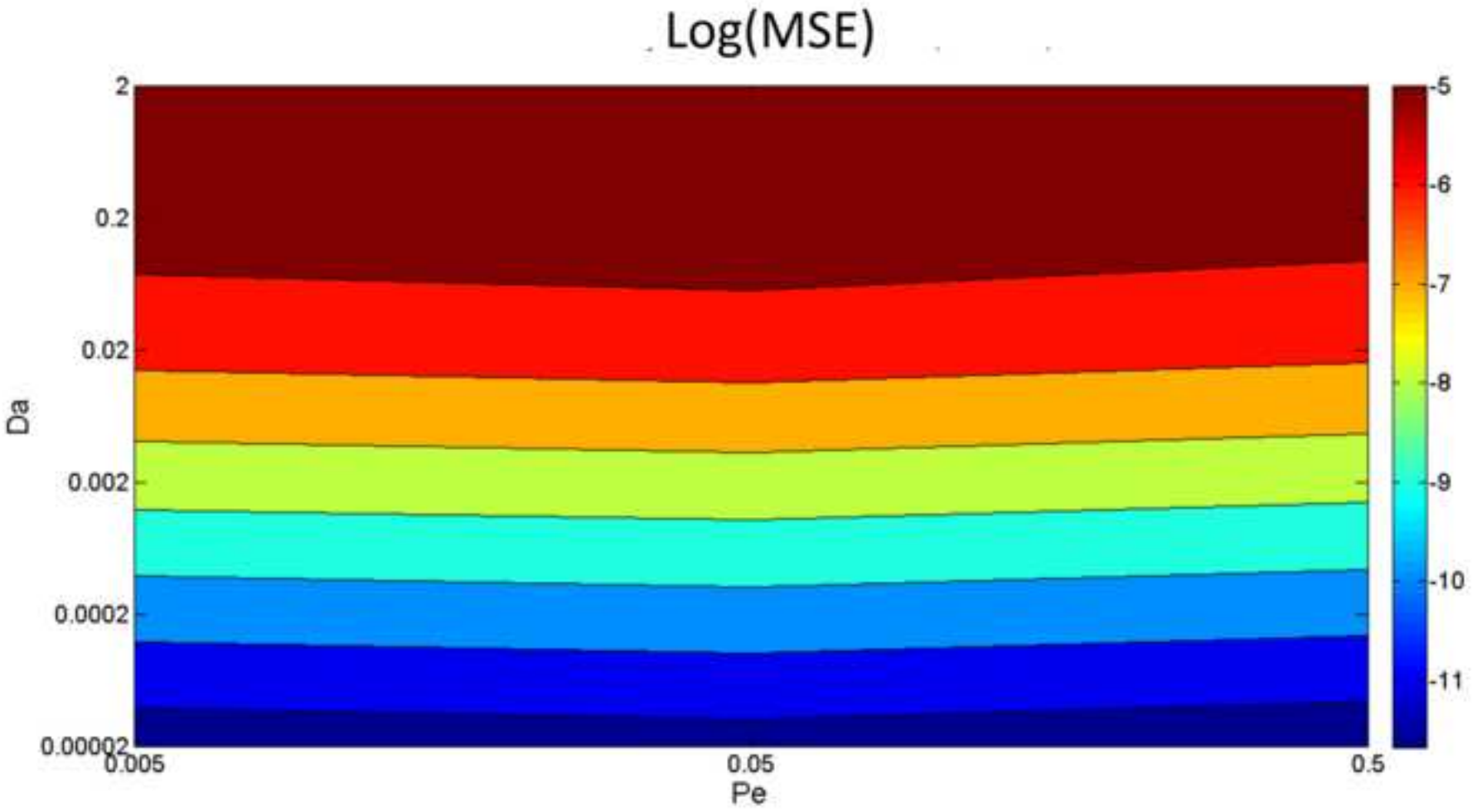

Figure 8

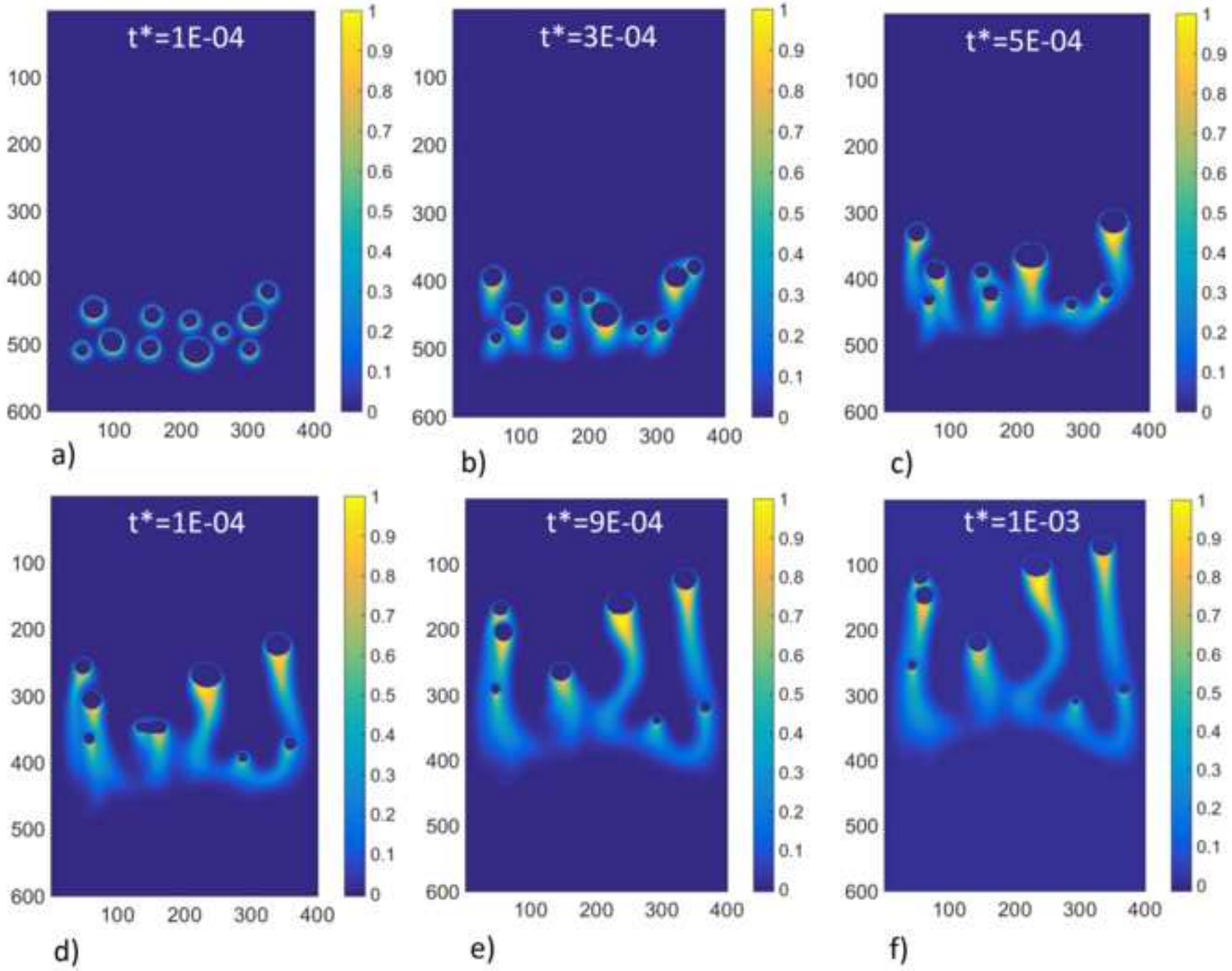

Highlights

A new lattice Boltzmann scheme for interface reaction is presented.

The Phase-field approach is used to identify the normal direction to the interface between two fluids and a new way to calculate the interface concentration is proposed.

Three different benchmark tests are presented to test the accuracy of the lattice Boltzmann model with analytical solutions.

A final simulation is performed coupling the lattice Boltzmann reactive model with a Shan Chen multiphase flow and computing the mass transfer across the interface by dissolution.